J. Fluid Mech. (2010), *vol.* 645, *pp.* 187–210. © Cambridge University Press 2010
doi:10.1017/S0022112009992631

Electro-hydrodynamic particle levitation on electrodes

EHUD YARIV†

Department of Mathematics, Technion – Israel Institute of Technology, Haifa 32 000, Israel

(Received 4 July 2009; revised 7 October 2009; accepted 7 October 2009)

The thin-Debye-layer model is utilized to analyse the electro-hydrodynamic flow about a colloidal particle which is exposed to a direct ionic current, emitted by a proximate reactive electrode. This flow is driven by electro-osmotic slip on the particle, as well as a comparable slip on the electrode itself. The small particle–electrode separation allows for the use of singular perturbation. Thus, the electro-neutral bulk-fluid domain is decomposed into an 'inner' gap region, where the electric field and shear rate are large, and an 'outer' region, consisting of the remaining bulk domain, where they are moderate. Matched asymptotic expansions in both regions provide the requisite flow field. The intensive shear rate in the narrow gap region is associated with a lubrication-type pressure build-up, which is responsible for the leading-order hydrodynamic force on the particle. This force acts to repel the particle away from the electrode, thereby supporting it against gravity. Its magnitude is inversely proportional to the gap width. At large distances from the particle the fluid velocity decays with the third power of distance, while near the electrode it decays with the fourth power. The inward pointing flow near the electrode tend to entrain neighbouring particles, thereby resulting in two-dimensional particle clusters. For equal values of particle and anode zeta potentials, this process is dominated by the particle-slip contribution.

1. Introduction

This paper is motivated by the observed interaction between colloidal particles that are electro-phoretically deposited on a planar electrode. After reaching the neighbourhood of the electrode, the initially dispersed particles appear to attract each other and to form two-dimensional crystalline aggregates (Böhmer 1996; Trau, Saville & Aksay 1996). This mode of guided self-assembly can be exploited for the fabrication of various nanostructured devices (Wong & Searson 1999), such as bio-sensors (Velev & Kaler 1999) and photonic crystals (Lumsdon *et al.* 2003). Accordingly, there is a significant practical interest in the aggregation dynamics. From a fundamental point of view, the clustering phenomenon presents a curious physical problem: Naively, the observed particle–particle attraction may appear surprising in view of the expected electrostatic repulsion between the identically charged particles. In reality, of course, the (usually negative) particle charge is screened by a thin diffuse layer, forming the electric double layer (Russel, Saville & Schowalter 1989). This suggests that the attraction mechanism is driven by electrokinetic effects (Böhmer 1996). Thus, the particles are entrained in an attractive fluid motion generated by

† Email address for correspondence: udi@technion.ac.il

https://doi.org/10.1017/S0022112009992631 Published online by Cambridge University Press

their neighbours. This effective attraction is arrested at short particle separation by repulsive dipole–dipole interactions (Gong & Marr 2001; Nadal *et al.* 2002), eventually resulting in the observed two-dimensional aggregates.

At the beginning of the aggregation process, the particles are well separated. Thus, an initial step in understanding particle interaction involves the study of the flow field which is caused by the interaction of a single particle with a proximate electrode. Once this flow field (and, specifically, its far-field behaviour) is reasonably understood, one can calculate the respective drift of a nearby 'test' particle using the existing models of particle mobility in the presence of walls (Goldman, Cox & Brenner 1967). The main interest therefore lies in the velocity distribution near the electrode, which is presumably the origin of inter-particle attraction.

1.1. *The electro-hydrodynamic and electro-osmotic mechanisms*

Two different electrokinetic mechanisms were actually proposed at about the same time. The 'electro-osmotic' mechanism, originally suggested by Böhmer (1996), is due to the flow which is engendered by the action of the electric field upon the diffuse layer which surrounds the particle. For the usual case of a negative particle zeta potential (positively charge diffuse layer), this mechanism predicts particle attraction near the anode. The 'electro-hydrodynamic' mechanism, on the other hand, is due to the flow driven by the action of the electric field upon the charged diffuse layer ('polarization layer') adjacent to the electrode itself. Since that layer is generated by the field, the electro-hydrodynamic mechanism is invariant to the electrodes polarity (for weakly applied voltage, for example, the flow magnitude is quadratic in the field). Thus, it generally predicts a velocity field along the electrode which is directed toward the particle, thereby resulting in particle–particle attraction. Another electro-hydrodynamic mechanism (Trau, Saville & Aksay 1997) is based upon the action of the electric field upon unbalanced charge outside the Debye layer. This mechanism was discussed in detail by Sides (2001).

The electro-osmotic mechanism accounts for many of the observed phenomena, and especially for aggregates disintegration at reversed electrode polarity under direct current (DC) conditions (Böhmer 1996). Being linear in the applied field, however, the electro-osmotic mechanism cannot explain alternating current (AC) aggregation. Recent experimental findings (Fagan, Sides & Prieve 2002), the most striking being the independence of the aggregation velocity upon the particle zeta potential (Kim *et al.* 2002*a*,*b*), indicate that the electro-osmotic mechanism alone may be insufficient to explain the clustering phenomena.

The electro-hydrodynamic mechanism, on the other hand, can explain particle attraction in both DC and AC conditions. Indeed, the early models of this mechanism (Sides 2001, 2003) are consistent with earlier AC experiments (Kim *et al.* 2002*a*). The existence of electro-hydrodynamic flow was later confirmed in kinetic experiments (Ristenpart, Aksay & Saville 2004). While there is no disagreement about the importance of the electro-hydrodynamic mechanism at high frequencies, the importance of this mechanism at low frequencies and at DC conditions is under debate (Solomentsev *et al.* 2000; Fagan, Sides & Prieve 2006)

Regardless of the assumed mechanism, prevailing analyses of this electrokinetic problem tend to consider a rather universal model geometry. Thus, a typical configuration comprises of a colloidal particle (radius a) which is suspended between two parallel planar electrode (spacing h) at distance $a\delta$ from the lower one (in DC models this is the anode). In typical experiments, h on the order of millimetres and a on the order of microns (see table 1). It is therefore common to focus upon the

https://doi.org/10.1017/S0022112009992631 Published online by Cambridge University Press

Electrochemical cell width	h	6 mm	(see e.g. Solomentsev *et al.* 1997)
Particle radius	a	10 μm	(see e.g. Solomentsev *et al.* 1997)
Particle–wall separation	$a\delta$	100 nm	(see e.g. Fagan *et al.* 2002)
Debye thickness	λ	20 nm	(see e.g. ristenpart *et al.* 2007*a*)

TABLE 1. Typical experimental values.

interaction of the particle with a single electrode, the other electrode being effectively replaced by a consistent far-field condition (see (2.7)). This transformation allows for the use of convenient analytical methods, such as bipolar coordinates (Solomentsev, Böhmer & Anderson 1997; Sides 2001), which naturally apply for the semi-infinite fluid domain.

1.2. *The thin-Debye-layer limit*

A key improvement of the modelling methods, pioneered by Solomentsev *et al.* (1997), exploited the smallness of the Debye layer thickness. Thus, the Debye layers on both the particle the electrode are effectively replaced by equivalent boundary conditions, which eliminate the need to solve the entire electrokinetic equations. These conditions consist of the Helmholtz–Smoluchowski slip formula (see (2.2)), as well as an appropriate condition for the electric field.

When considering a chemically inert particle, the impermeability of the particle to ionic current is reflected by a no-flux condition (Keh & Anderson 1985; Yariv 2010). On the reactive electrode, however, the choice of appropriate boundary condition has resulted in some controversy. Original investigations of the particle–electrode interaction employed a constant potential boundary condition (Reed & Morrison 1976; Keh & Anderson 1985; Keh & Lien 1989; Loewenberg & Davis 1995; Solomentsev *et al.* 1997). Since this condition does not allow for electrokinetic slip on the electrode, it rules out the electro-hydrodynamic mechanism. It was later realized (Fagan, Sides & Prieve 2004) that the constant potential condition is applicable on the Debye layer scale, but is inappropriate for a coarse-grained bulk description in a thin-Debye-layer limit. The first thin-Debye-layer model of a reactive electrode appears to be that of Fagan *et al.* (2004), who considered the case of low AC frequencies, wherein Faradaic reactions occur at the electrodes. Rather than using a constant potential condition, the authors postulated a constant reaction rate at the electrode.

In the DC case, this simplifying methodology was continued by Ristenpart, Aksay & Saville (2007*a*). These authors extended their analysis beyond any specific kinetic model by assuming a *prescribed* current density on the reactive electrodes. (This condition constitutes the natural counterpart of the familiar no-flux condition on inert surfaces.) Thus, while the current density depends upon the applied voltage through the electrodes kinetics, the approach of Ristenpart *et al.* (2007*a*) consists of ignoring the electrochemical details and focusing upon the hydrodynamics. Using the ensuing non-homogeneous Neumann condition, Ristenpart *et al.* (2007*a*) managed to obtain a semi-analytical solution of the electric field as an eigenfunction series in bi-polar coordinates. In a companion paper (Ristenpart, Aksay & Saville 2007*b*) the same authors addressed the high-frequency AC case, in the absence of any Faradaic reactions.

1.3. *The near-contact limit*

A common feature in the observed phenomenon is the small gap separating the particle from the electrode. In the height-tracking experiments of Fagan *et al.* (2002), for example, the 6.2 μm diameter particles were observed at distances of order 0.1 μm

https://doi.org/10.1017/S0022112009992631 Published online by Cambridge University Press

from the electrode (see table 1). Consequently, numerical solutions of the theoretical models (Solomentsev *et al.* 1997, 2000; Sides 2003; Fagan *et al.* 2004; Ristenpart *et al.* 2007*a*,*b*) consistently employed small numerical values of δ, e.g. 0.04 in Ristenpart *et al.* (2007*a*) and 0.01 in Ristenpart *et al.* (2007*b*). These figures represent separations that are small compared with particle size, yet large relative to the Debye thickness, $\lambda \ll a\delta \ll a$. This scale disparity allows for the use of the thin-Debye-layer models even for these small separations. Surprisingly, it appears that none of the many existing models has directly exploited the smallness of δ to obtain an asymptotic approximation for the flow field. Indeed, it appears that the only direct use of the small-δ values was made by Solomentsev *et al.* (2000) who employed the well-known asymptotic model for near-contact wall hindrance.

The goal of the present paper is to present an asymptotic analysis for the near-contact limit $\delta \ll 1$. In contrast to the comparable numerical solutions, this analysis provides closed-form expressions for the electric and flows fields, and, specifically, for the flow distribution along the electrode. Extracting to large distances away from the particle, this distribution is utilized to calculate the drift of a neighbouring particle which is entrained in that flow. Thus, the present analysis clarifies the relative role of the electro-hydrodynamic mechanism in DC aggregation, thereby aiding in resolving a long-standing dispute. An additional important benefit of the asymptotic solution is in providing a physical explanation for the lubrication-type support that is required to balance the particle against gravity. As will become evident here, this support arises from the large pressure in the gap region.

The paper is arranged as follows: the next section provides the thin-Debye-layer formulation and presents the near-contact limit, whereby inner–outer asymptotic expansions are utilized for analysing the problem separately in the gap region and in the remaining fluid domain. Section 3 presents the calculation of the electric field in both regions, thereby allowing for the evaluation of the slip-driven velocity field. The electro-hydrodynamic flow associated with the electrode diffuse layer is calculated in § 4, and the electro-osmotic flow associated with the particle diffuse layer is calculated in § 5. The predictions of the present theory for particle–particle interactions and the hydrodynamic force experienced by the particle are provided in § 6. The results are discussed in § 7.

2. Problem formulation

2.1. *Model*

Consider an electrochemical cell consisting of two planar electrodes separated by distance h (see figure 1). The space between the electrodes is filled with an electrolyte solution (permittivity ϵ, viscosity μ). For simplicity, a symmetric solution (cation valency $\mathscr{Z}$, anion valency $-\mathscr{Z}$) is assumed, so when undisturbed both ionic species possess identical ionic concentration, say n_∞. As in Ristenpart *et al.* (2007*a*), the focus here is on the case of a DC which is generated by electrochemical reactions that take place on the electrode-electrolyte interfaces. Following Ristenpart *et al.* (2007*a*), these reactions are modelled by a prescribed current density, flowing out of the anode.

It is instructive to consider first the transport process in the absence of a particle. Then, the system is one-dimensional, whereby charge conservation implies that the current density I must be uniform in the entire cell. Despite the passage of this ionic current through the cell, the electrolyte remains electro-neutral to leading order. Neglecting the effect of concentration polarization (Rubinstein & Zaltzman 2001), which is expected to be secondary in the electrode neighbourhood, this electro-neutrality

https://doi.org/10.1017/S0022112009992631 Published online by Cambridge University Press

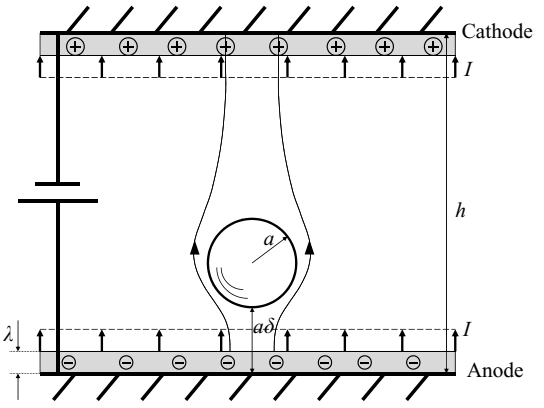


FIGURE 1. Schematic of the electrodes–particle system, showing the oppositely charged diffuse layers near the electrodes. In the thin-Debye-layer limit $\lambda/a \to 0$, the Debye layer adjacent to the anode is assumed to be quantified by a zeta potential ζ and a uniform Faraday current density I.

implies that both ionic concentrations are equal to n_∞, whereby the electrolyte behaves as an Ohmic conductor of a uniform conductivity, say σ. Thus, for example, if both ionic species possess the same diffusivity D,

$$\sigma = \frac{2\mathrm{e}^2 \mathscr{Z}^2 n_\infty D}{kT}, \tag{2.1}$$

wherein kT denotes Boltzmann's factor and e the elementary charge.

Electro-neutrality is violated only in the diffuse layers adjacent to the two electrodes. Since the Debye layer thickness λ is on the order of nanometres in most practical scenarios, both diffuse layers can be modelled using the thin-Debye-layer limit. Thus, for instance, the anode is quantified by a positive zeta potential, say ζ, representing the voltage across the negative Debye cloud surrounding it. The values of I and ζ are (in general nonlinear) functions of the imposed voltage, the electrode kinetics, and the cell separation h (Bazant, Chu & Bayly 2005). In principle, these functions can be obtained for any electrode kinetic model; in the case of transport through ideal ion-selective membranes, for example, the current increases monotonically as the hyperbolic tangent of V, exponentially approaching a saturation plateau (Levich 1962).

Consider now the effect of a stationary colloidal particle of radius a which is suspended at distance $a\delta$ from the anode. In view of the particle impermeability to ions, the preceding one-dimensional solution is no longer valid, and it is necessary to analyse the spatial transport problem. The smallness of a compared with h allows for representing the remote cathode by an equivalent far-field condition (see (2.7)). Within the thin-Debye-layer limit (Keh & Anderson 1985; Yariv 2010), the particle boundary is represented by a current-impermeability boundary condition, implying that the current distribution is modified and is no longer one-dimensional. (At large zeta potentials, comparable to the thermal voltage, this no-flux condition needs to be corrected so as to account for the emergence of surface current (Dukhin 1965; O'Brien 1983). Since the goal here is to employ the simplest model which exhibits all the essential electrokinetics features, the conventional no-flux condition is employed. This is the only place where the present thin-Debye-layer model departs from that of Ristenpart *et al.* (2007*a*).)

https://doi.org/10.1017/S0022112009992631 Published online by Cambridge University Press

It is important to emphasize that consistent use of the thin-Debye-layer limit implies now that the asymptotic condition $\lambda \ll h$ is replaced by the stricter condition $\lambda \ll a\delta$. This assumption is justified by the existing length disparities in realistic systems (see table 1). Thus, all pertinent fields are sought in the electro-neutral bulk domain, external to the Debye layers surrounding both the particle and the electrodes. This bulk behaves approximately as an Ohmic conductor, wherein the (now non-uniform) current density is related to the electric field through the scalar conductivity σ. Within the thin-Debye-layer limit, this field results in the Helmholtz–Smoluchowski velocity slip,

$$\text{slip} = -\frac{\epsilon}{\mu} \times \text{electric field} \times \text{zeta potential}, \tag{2.2}$$

over all charged surfaces in contact with the electrolyte. Consistently with the thin-Debye-layer limit, the effective boundary condition apply at the outer edges $\mathscr{E}$ and $\mathscr{P}$ of the diffuse layers that surround the electrode and particle, respectively. (At the bulk scale, these surfaces coincide with the electrode surface and particle boundary.)

Thus, the introduction of an ion-impermeable particle into the system results in a non-uniform electric current (and electric field) in the electro-neutral bulk. This field, in turn, induces velocity slip on both the anode and the particle, the magnitude of which is provided by (2.2). The usual assumption of a uniform (usually negative) zeta potential ζ_P on the particle, as would be the case for a latex particle, is employed.

2.2. *A simplified electrode representation*

In the absence of a particle, both the current distribution on the electrode and the electrode zeta potential are uniform. In principle, these two quantities depend upon both the applied voltage across the cell, as well as the electrode kinetics (Bazant *et al.* 2005). Adopting the approach of Ristenpart *et al.* (2007*a*), both quantities are taken as prescribed, thereby ignoring the electrochemical details.

When the particle is introduced into the cell, the transport process is no longer one-dimensional, whereby the distributions of current and zeta potential on the electrode may deviate from their original uniform values. Following Ristenpart *et al.* (2007*a*), however, these deviations are neglected. Thus, the electrode is represented by a uniform current density I and zeta potential ζ. The assumption of a uniform electrode current is valid provided the Ohmic resistance in the bulk is small compared with the electrochemical charge-transfer resistance at the electrode–electrolyte interface (Newman 1973); this is indeed the case in typical experiments (Sides 2001). The assumption of uniform zeta potential is justified if the characteristic electric potential variations in the bulk fluid, of order aI/σ, are small compared with the kinetic-driven voltage drop across the electrode Debye layer.

Both approximation may become somewhat crude as the particle approaches the electrode, and especially in the near-contact limit considered here. Specifically, it is anticipated that the intensification of electric field would result in induced-charge effects, whereby the zeta potential may be significantly affected by the electric potential distribution in the bulk (Bazant & Squires 2004; Squires & Bazant 2004).

A rigorous evaluation of the current density and zeta potential distributions requires a careful asymptotic analysis, where these two macroscale quantities are calculated form an exact microscale description. This problem was recently resolved for one-dimensional transport (Bazant *et al.* 2005); its generalization to more complicated geometries is discussed in § 7.

https://doi.org/10.1017/S0022112009992631 Published online by Cambridge University Press

2.3. *Electrostatics*

The electrostatic problem is analysed using a dimensionless formulation, where the spatial coordinates are normalized with a, the current density with I, the electric potential with aI/σ and the electric field with I/σ. The Ohmic nature of the electroneutral bulk implies that the dimensionless current $\boldsymbol{i}$ and the dimensionless electric field coincide; because of Maxwell–Faraday law, the latter is conservative, whence

$$\boldsymbol{i} = -\nabla\varphi, \tag{2.3}$$

where φ is the electric potential. Charge conservation then yields Laplace's equation:

$$\nabla^2\varphi = 0. \tag{2.4}$$

The dimensionless boundary conditions are formulated using a cylindrical (ρ, ϖ, z) coordinate system, the z-axis passing through the particle centre and lying perpendicular to the electrodes, in addition to spherical polar coordinates r and θ (see figure 3). The prescribed uniform current density on the anode surface $z = 0$ appears as the Neumann-type boundary condition

$$\frac{\partial\varphi}{\partial z} = -1 \quad \text{on} \quad \mathscr{E}. \tag{2.5}$$

Similarly, the particle impermeability to current is expressed via the no-flux condition

$$\frac{\partial\varphi}{\partial n} = 0 \quad \text{on} \quad \mathscr{P}, \tag{2.6}$$

where $\partial/\partial n$ denotes differentiation along the outward normal to the particle boundary. The remote cathode is represented by the far-field condition

$$\frac{\partial\varphi}{\partial z} = -1 \quad \text{as} \quad z \to \infty. \tag{2.7}$$

Owing to the axial symmetry of the problem, φ is a function of ρ and z alone, independent of the azimuthal angle ϖ.

2.4. *Flow*

Since the flow is driven by the Smoluchowski slip condition (2.2), it is natural to normalize the velocity field with the electrokinetic scale (see (2.1)):

$$\mathscr{U} = \frac{\epsilon\zeta I}{\sigma\mu}. \tag{2.8}$$

The pressure is normalized with $\mu\mathscr{U}/a$. The dimensionless velocity $\boldsymbol{v}$ and pressure p are governed by the continuity and Stokes equations,

$$\nabla\cdot\boldsymbol{v} = 0, \quad \nabla p = \nabla^2\boldsymbol{v}, \tag{2.9}$$

together with the attenuation condition

$$\boldsymbol{v} \to \boldsymbol{0} \quad \text{for} \quad z \to \infty. \tag{2.10}$$

In addition, the velocity field satisfies mass impermeability and electrokinetic slip on the electrode surface:

$$\boldsymbol{v} = \nabla\varphi \quad \text{on} \quad \mathscr{E}, \tag{2.11}$$

and on the particle boundary:

$$\boldsymbol{v} = \chi\nabla\varphi \quad \text{on} \quad \mathscr{P}. \tag{2.12}$$

https://doi.org/10.1017/S0022112009992631 Published online by Cambridge University Press

Here,

$$\chi = \zeta_P/\zeta \tag{2.13}$$

is the ratio of particle to electrode zeta potentials.

In view of the linearity of the hydrodynamic problem, it is convenient to decompose the velocity field in the form

$$\boldsymbol{v} = \boldsymbol{u} + \chi\tilde{\boldsymbol{u}}, \tag{2.14}$$

the pressure field is similarly decomposed to $p + \chi\tilde{p}$. Hereafter, the flow fields $(\boldsymbol{u}, p)$ and $(\tilde{\boldsymbol{u}}, \tilde{p})$ are respectively referred to as the 'electro-hydrodynamic' and 'electro-osmotic' components. Both fields independently satisfy the continuity and Stokes equations (2.9) as well as the decay condition (2.10). The field $\boldsymbol{u}$, which represents the motion due to the electrode slip, vanishes on $\mathscr{P}$ and satisfies

$$\boldsymbol{u} = \nabla\varphi \quad \text{on} \quad \mathscr{E}, \tag{2.15}$$

while the field $\tilde{\boldsymbol{u}}$, which represents the motion due to the particle slip, vanishes on $\mathscr{E}$ and satisfies

$$\tilde{\boldsymbol{u}} = \nabla\varphi \quad \text{on} \quad \mathscr{P}. \tag{2.16}$$

In view of the prevailing axial symmetry, $\boldsymbol{u}$ comprises only of radial (u) and axial (w) components when written in cylindrical coordinates:

$$\boldsymbol{u} = \hat{\boldsymbol{e}}_\rho u + \hat{\boldsymbol{e}}_z w \tag{2.17}$$

wherein $\hat{\boldsymbol{e}}_\rho$ and $\hat{\boldsymbol{e}}_z$ are unit vectors in the directions of increasing ρ and z, respectively. These two components, moreover, are functions of ρ and z alone, independent of ϖ. That symmetry allows to express these components in terms on a stream function ψ:

$$u = \frac{1}{\rho}\frac{\partial\psi}{\partial z}, \quad w = -\frac{1}{\rho}\frac{\partial\psi}{\partial\rho}, \tag{2.18}$$

whereby the continuity equation is automatically satisfied. A similar representation also applies for $\tilde{\boldsymbol{u}} = \hat{\boldsymbol{e}}_\rho\tilde{u} + \hat{\boldsymbol{e}}_z\tilde{w}$, wherein both $\tilde{u}$ and $\tilde{w}$ can be derived from a stream function $\tilde{\psi}$ using relations of the form (2.18).

2.5. *The near-contact limit*

The focus here is in the prevailing case where the particle–electrode gap is narrow, $\delta \ll 1$. This singular limit is handled by decomposing the fluid domain into two complementary regions: an 'inner' gap region, where the electric field and shear rate are presumably intensive, and the 'outer' region, consisting of the remaining fluid domain, where they are moderate. The gap region is analysed using the standard lubrication variable stretching (Keller 1963):

$$z = \delta Z, \quad \rho = \delta^{1/2}R, \tag{2.19}$$

whereby the lower particle hemisphere appears as

$$Z \sim H_0(R) + \delta H_1(R) + \cdots = H(R;\delta) \tag{2.20}$$

with

$$H_0(R) = 1 + \frac{1}{2}R^2. \tag{2.21}$$

In the outer region, the limit $\delta \to 0$ corresponds at leading order to a unit sphere in contact with planar wall. This geometry is naturally resolved using tangent-sphere

https://doi.org/10.1017/S0022112009992631 Published online by Cambridge University Press

coordinates (ξ, ϖ, η) (Jeffrey 1978; Sides & Tobias 1980):

$$\rho = \frac{2\eta}{\xi^2 + \eta^2}, \qquad z = \frac{2\xi}{\xi^2 + \eta^2}, \tag{2.22}$$

in which the spheres $\xi =$ constant are centreed about the point $\xi^{-1}\hat{\boldsymbol{e}}_z$ and are tangential to the $z = 0$ plane. In terms of these coordinates the wall is located at $\xi = 0$, whereas the sphere surface is given to leading order by $\xi = 1$.

3. Electric field

The electrokinetic problem is semicoupled: while the hydrodynamic problem depends upon the electric flow trough the slip conditions (2.11)–(2.12), the electrostatic problem can be analysed independently. This section is devoted to the calculation of the electric field in both the inner and outer regions.

3.1. *Inner region*

In terms of the inner variables, Laplace's equation adopts the form

$$\frac{\partial^2 \varphi}{\partial Z^2} + \delta\left(\frac{\partial^2 \varphi}{\partial R^2} + \frac{1}{R}\frac{\partial \varphi}{\partial R}\right) = 0; \tag{3.1}$$

the Faraday current condition (2.5) on $\mathscr{E}$ appears as

$$\frac{\partial \varphi}{\partial Z} = -\delta \quad \text{on} \quad Z = 0, \tag{3.2}$$

and the no-flux condition (2.6) on $\mathscr{P}$ is given by

$$\frac{\partial \varphi}{\partial Z} = \delta \frac{\mathrm{d}H}{\mathrm{d}R}\frac{\partial \varphi}{\partial R} \quad \text{at} \quad Z = H. \tag{3.3}$$

For $\delta \ll 1$ is is natural to seek a solution in the form of an asymptotic expansion

$$\varphi(R, Z; \delta) \sim f_0(\delta)\varphi_0(R, Z) + f_1(\delta)\varphi_1(R, Z) + \cdots, \tag{3.4}$$

wherein $f_i(\delta)$ is an asymptotic sequence:

$$f_{i+1}(\delta) \ll f_i(\delta), \quad \delta \to 0. \tag{3.5}$$

Specifically, in view of the structure (3.1)–(3.3), it appears natural to choose

$$f_0(\delta) = 1, \quad f_1(\delta) = \delta, \quad \ldots. \tag{3.6}$$

The leading-order balance yield $\partial\varphi_0/\partial Z = 0$, whence $\varphi_0 = \varphi_0(R)$. (This result, in conjunction with (3.6), implies an $O(\delta^{-1/2})$-large radial current.). The function φ_0 is evaluated from the solvability condition of the $O(\delta)$ problem:

$$\frac{\partial^2 \varphi_1}{\partial Z^2} = -\frac{1}{R}\frac{\mathrm{d}}{\mathrm{d}R}\left(R\frac{\mathrm{d}\varphi_0}{\mathrm{d}R}\right), \tag{3.7}$$

$$\frac{\partial \varphi_1}{\partial Z} = -1 \quad \text{on} \quad Z = 0, \tag{3.8}$$

$$\frac{\partial \varphi_1}{\partial Z} = \frac{\mathrm{d}H_0}{\mathrm{d}R}\frac{\mathrm{d}\varphi_0}{\mathrm{d}R} \quad \text{at} \quad Z = H_0. \tag{3.9}$$

Integration of (3.7) in conjunction with (3.8) yields

$$\frac{\partial \varphi_1}{\partial Z} = -1 - \frac{Z}{R}\frac{\mathrm{d}}{\mathrm{d}R}\left(R\frac{\mathrm{d}\varphi_0}{\mathrm{d}R}\right). \tag{3.10}$$

https://doi.org/10.1017/S0022112009992631 Published online by Cambridge University Press

The no-flux condition (3.9) then furnishes the equation:

$$\frac{H_0}{R}\frac{\mathrm{d}}{\mathrm{d}R}\left(R\frac{\mathrm{d}\varphi_0}{\mathrm{d}R}\right)+R\frac{\mathrm{d}\varphi_0}{\mathrm{d}R}+1=0. \tag{3.11}$$

This is a first-order differential equation for $\mathrm{d}\varphi_0/\mathrm{d}R$ whose solution is

$$\frac{\mathrm{d}\varphi_0}{\mathrm{d}R}=\frac{C_0}{RH_0}-\frac{1}{R}, \tag{3.12}$$

where C_0 is a constant of integration. Preventing field singularity at $R=0$ requires that $C_0=1$, whence

$$\frac{\mathrm{d}\varphi_0}{\mathrm{d}R}=-\frac{R}{2H_0(R)}. \tag{3.13}$$

This expression can also be obtained using integral charge conservation in a region of radius R (cf. Jeffrey & Chen 1977): the current that enters this region from the anode $\pi\delta R^2$ must be balanced by a radial current, which to leading order is $-2\pi\delta R H_0(R)\,\mathrm{d}\varphi_0/\mathrm{d}R$. This yields (3.13). (At first sight, it may appear surprising that the integral method automatically yields (3.12) with $C_0=1$ without the need to employ the regularity condition at $R=0$. Note however that, for any $C_0\neq 1$, (3.12) comprises a singular current source term which is not accounted by the integral balance.) In the present context, the direct method used herein is necessary as it provides the boundary value problem governing φ_1 which is required in subsequent flow analysis (see (5.2)).

To conclude, the inner potential is

$$\varphi_0=D_0-\frac{1}{2}\ln H_0. \tag{3.14}$$

The integration constant D_0 is obtained by matching with the outer solution.

3.2. *Outer field*

Consider now the outer region. It is convenient here to decompose the potential as

$$\varphi=-z+\phi, \tag{3.15}$$

ϕ representing the modification to the uniform current due to the particle, decaying at large distances (cf. (2.7)):

$$\phi\to 0 \quad \text{as} \quad \xi,\eta\to 0. \tag{3.16}$$

As such, ϕ satisfies Laplace's equation, the homogeneous no-flux condition at the wall (cf. (2.5))

$$\frac{\partial\phi}{\partial\xi}=0 \quad \text{at} \quad \xi=0 \tag{3.17}$$

and an attenuation condition. Additionally, it satisfies a non-homogeneous boundary condition on the sphere surface (cf. (2.6)):

$$\frac{\partial\varphi}{\partial n}=\frac{\partial z}{\partial n} \quad \text{on} \quad \mathscr{P}. \tag{3.18}$$

The modification ϕ is expanded into the asymptotic series:

$$\phi(\xi,\eta;\delta)\sim\phi_0(\xi,\eta)+\delta\,\phi_1(\xi,\eta)+\cdots. \tag{3.19}$$

The leading-order term satisfies both Laplace's equation and the homogeneous condition (3.17). In addition, it satisfies the following non-homogeneous boundary

https://doi.org/10.1017/S0022112009992631 Published online by Cambridge University Press

condition on the sphere surface (cf. (3.18)):

$$\frac{\partial \phi_0}{\partial \xi} = 2\frac{\eta^2 - 1}{(\eta^2 + 1)^2} \quad \text{at} \quad \xi = 1. \tag{3.20}$$

The axisymmetric solution of Laplace's equation that satisfies (3.17)–(3.16) is (Moon & Spencer 1988)

$$\phi_0 = (\xi^2 + \eta^2)^{1/2} \int_0^\infty A(s)\, \cosh(\xi s)\, J_0(\eta s)\, \mathrm{d}s. \tag{3.21}$$

Substitution into (3.20) in conjunction with the properties of the Hankel transforms (Sneddon 1972) leads to the following first-order ordinary differential equation for $\mathrm{d}A/\mathrm{d}s$:

$$s\, \sinh s\, \frac{\mathrm{d}^2 A}{\mathrm{d}s^2} + (\sinh s + 2s \cosh s)\frac{\mathrm{d}A}{\mathrm{d}s} = -2(1 - 2s)\mathrm{e}^{-s}. \tag{3.22}$$

Integration yields

$$\frac{\mathrm{d}A}{\mathrm{d}s} = \frac{4\mathrm{e}^{2s}(\mathrm{e}^{-2s} - 1 + s)}{(\mathrm{e}^{2s} - 1)^2} + \frac{C\mathrm{e}^{2s}}{s(\mathrm{e}^{2s} - 1)^2}. \tag{3.23}$$

For small s, the first term $\sim -1/s$ while the second term $\sim C/4s^3$. Convergence of (3.21) therefore requires $C = 0$. Another integration yields

$$A(s) = E - \frac{s\mathrm{e}^{-s}}{\sinh s} - \ln(1 - \mathrm{e}^{-2s}). \tag{3.24}$$

Convergence of (3.21) therefore requires $E = 0$. (A different solution, appearing in Jeffrey & Chen (1977) for a similar potential-flow problem, does not satisfy their differential equation and is erroneous.) Note that at small s

$$A(s) \sim -\ln s - 1 - \ln 2 + O(s). \tag{3.25}$$

When approaching the gap region, as $\eta \to \infty$, the main contribution to the integral in (3.21) arises from the $s = O(1/\eta)$ neighbourhood; use of (3.25) readily yields

$$\phi_0 \sim \ln \eta + \gamma - 1 + O(1/\eta), \tag{3.26}$$

γ being Euler's constant. Performing a 1–1 van Dyke matching (Van Dyke 1964) reveals that the integration constant in the leading-order inner potential (3.14) is

$$D_0 = \frac{1}{2}\ln 2 + \gamma - 1. \tag{3.27}$$

It also shows a *switchback* effect (Hinch 1991), whereby the inner expansion (3.4) is modified to

$$\varphi(R, Z; \delta) \sim f_{-1}(\delta)\varphi_{-1}(R, Z) + f_0(\delta)\varphi_0(R, Z) + f_1(\delta)\varphi_1(R, Z) + \cdots, \tag{3.28}$$

wherein

$$f_{-1}(\delta) = \ln \delta \tag{3.29}$$

and $\varphi_{-1} = -1/2$. Since φ_{-1} is a constant, it is readily verified that the modification (3.28) does not affect the validity of the preceding inner analysis.

It is worth noticing that the electric potential is defined to within an additive constant, which is set here by (3.15)–(3.16). Thus, the constants of integration in the inner solution are not arbitrary, but must rather be determined by matching with the outer solution. In the thin-Debye-layer model of Ristenpart *et al.* (2007*a*)

https://doi.org/10.1017/S0022112009992631 Published online by Cambridge University Press

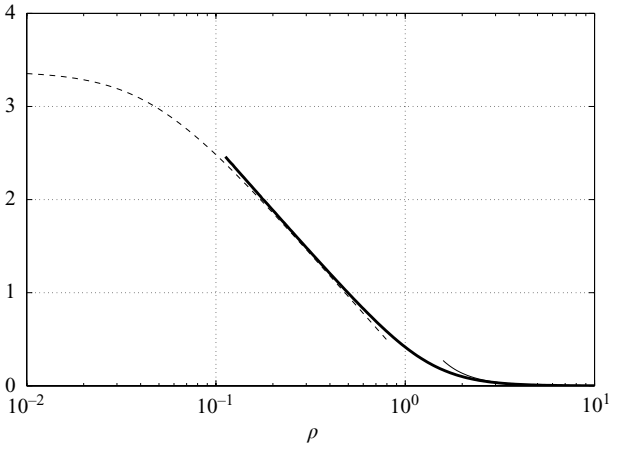


FIGURE 2. The electric potential at $z = 0$ as a function of ρ for $\delta = 0.001$: outer approximation ϕ_0 (thick), inner approximation $\varphi_{-1} \ln \delta + \varphi_0$ (dashed) and remote approximation $\pi^4/90\rho^3$ (thin).

the electrode zeta potential is assumed uniform, presumably unaffected by the bulk-electric-potential variations at $z = 0$; then, the flow problem is only affected by the local gradient of φ, thereby unaffected by both D_0 and the switchback term. In a more realistic model, however, the zeta potential would be affected by the actual distribution of $\varphi(z = 0)$ (see Yariv 2008).

The representation (3.21) enables the derivation of an asymptotic approximation at large distances from the particle. Evaluating the integral in (3.21) for $\eta, \xi \ll 1$ and reverting to outer variables reveals that ϕ_0 is given by a quadrupole aligned in the z direction. In spherical coordinates,

$$\phi_0 \sim -\frac{\pi^4}{90}\frac{3\cos^2\theta - 1}{r^3}. \tag{3.30}$$

This approximation corresponds to an outward current near the electrode ($\arccos(1/3) < \theta < \pi/2$) and an inward current near the symmetry axis ($0 < \theta < \arccos(1/3)$). Note that the total current associated with (3.30) through any hemisphere ($r = \text{const.}$) is zero, in agreement with the physical interpretation of ϕ as a disturbance caused by the particle.

The electric potential distribution on the anode is portrayed in figure 2. The thick line represents the leading-order outer approximation ϕ_0, obtained using (3.21) and (3.24). The thin line at large ρ values represents the remote approximation (3.30). The dashed line at small ρ values represents the leading-order inner approximation, $-\ln(\delta H_0)/2$. Following van Dyke (1964), the latter approximation comprises both the logarithmic and $O(1)$ terms in (3.28).

4. Flow due to electrode-animated slip

Having evaluated the electric field, it is now possible to calculate the electrokinetic flow using the decomposition (2.14). The electro-hydrodynamic velocity field, due to slip over the electrode Debye layer, is calculated first.

4.1. *Inner region*

Consider first the flow field in the gap. The slip condition (2.15) in conjunction with (3.4) implies $O(\delta^{-1/2})$ radial velocities; the continuity equation in conjunction with

https://doi.org/10.1017/S0022112009992631 Published online by Cambridge University Press

mass impermeability at both the electrode and particle surface then implies $w \sim O(1)$. Balancing the radial pressure gradient with the large viscous stresses associated with the transverse variation of u shows that the pressure is $O(\delta^{-2})$. This suggests the introduction of the lubrication scaling:

$$u = \delta^{-1/2}U, \quad w = W, \quad p = \delta^{-2}P. \tag{4.1}$$

Consequently, it also useful to define

$$\psi = \delta\Psi, \tag{4.2}$$

wherein (cf. (2.18))

$$U = \frac{1}{R}\frac{\partial\Psi}{\partial Z}, \quad W = -\frac{1}{R}\frac{\partial\Psi}{\partial R}. \tag{4.3}$$

The scaling (4.1) is identical to that obtained by Cox & Brenner (1967) for the classical Stokes problem of a sphere approaching a solid wall. In that problem, however, the flow is driven by the $O(1)$ axial velocity imposed by the sphere motion; in the present case the flow is driven by the slip-driven $O(\delta^{-1/2})$ radial velocity.

Each of the fields U, W, P and Ψ is expanded in the form (3.4). At leading order, the continuity equation appears as

$$\frac{\partial W_0}{\partial Z} + \frac{1}{R}\frac{\partial}{\partial R}(RU_0) = 0, \tag{4.4}$$

while the radial and axial components of Stokes equation are

$$\frac{\partial P_0}{\partial R} = \frac{\partial^2 U_0}{\partial Z^2}, \quad \frac{\partial P_0}{\partial Z} = 0. \tag{4.5}$$

The last equation implies that P_0 is independent of Z, $P_0 = P_0(R)$. The axial component W_0 vanishes on both $Z = 0$ and on the surface $Z = H_0(R)$; the radial component U_0 also vanishes on that surface, but on $Z = 0$ it satisfies the condition,

$$U_0 = \frac{\mathrm{d}\varphi_0}{\mathrm{d}R} \quad \text{at} \quad Z = 0, \tag{4.6}$$

representing the electro-hydrodynamic slip along the outer edge of the anode diffuse layer.

Integrating the radial momentum balance in conjunction with the boundary conditions governing U_0 yields

$$U_0 = \frac{R}{2H_0^2}(Z - H_0) + \frac{1}{2}\frac{\mathrm{d}P_0}{\mathrm{d}R}Z(Z - H_0). \tag{4.7}$$

The first term represent an inward Couette-like radial flow, driven by electrode slip; the second term represents Poiseuille-type radial flow that is required by mass conservation (see figure 3).

With the available expression for U_0, it is trivial to evaluate W_0 from the continuity equation (4.4). Applying the boundary condition at $Z = 0$ and $Z = H_0$ results in the following first-order differential equation for $\mathrm{d}P_0/\mathrm{d}R$:

$$H_0^3\frac{\mathrm{d}}{\mathrm{d}R}\left(R\frac{\mathrm{d}P_0}{\mathrm{d}R}\right) + 3H_0^2R^2\frac{\mathrm{d}P_0}{\mathrm{d}R} = -6R. \tag{4.8}$$

The left-hand side of (4.8) is the derivative of $H^3R\,\mathrm{d}P_0/\mathrm{d}R$; integration yields

$$\frac{\mathrm{d}P_0}{\mathrm{d}R} = -3\frac{R}{H_0^3} + \frac{E_0}{RH_0^3}, \tag{4.9}$$

https://doi.org/10.1017/S0022112009992631 Published online by Cambridge University Press

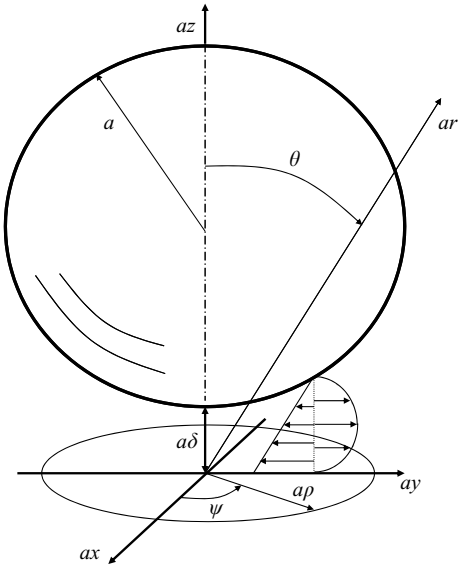


FIGURE 3. A description of the cylindrical and spherical coordinates systems. Also depicted is the electro-hydrodynamic flow field in the gap. The Couette and Poiseuille velocity profiles respectively correspond to the first and second terms in (4.7).

where E_0 is a constant of integration. The second term results in a logarithmic singularity of P near $R = 0$ and is therefore rejected, whence $E_0 = 0$. A second integration yields

$$P_0 = \frac{3}{2H_0^2}. \tag{4.10}$$

The constant of integration in the above expression was set to zero in view of the required matching with the $O(1)$ pressure in the outer region.

Thus, the outward Poiseuillian flow, which is induced by mass conservation, is accompanied by large pressure buildup in the gap. Note that this mechanism is independent of the electrode polarity: at the cathode, the electric current inflow is accompanied by large inward radial current, namely the opposite of (3.13). The zeta potential, however, is then negative, and the animating slip is again in the inward radial direction.

The inner flow calculation is summarized by presenting the leading-order stream function, obtained from (4.3), (4.7) and (4.9):

$$\Psi_0 = -\frac{R^2 Z(H_0 - Z)^2}{2H_0^3}. \tag{4.11}$$

4.2. *Outer region*

Consider now the electro-hydrodynamic flow in the outer region. The respective stream function ψ (defined by (2.18)) is governed by the Stokes equation

$$\left(\frac{\partial^2}{\partial\rho^2} - \frac{1}{\rho}\frac{\partial}{\partial\rho} + \frac{\partial^2}{\partial z^2}\right)^2 \psi = 0, \tag{4.12}$$

https://doi.org/10.1017/S0022112009992631 Published online by Cambridge University Press

the impermeability and slip conditions on the electrode

$$\psi = 0, \quad \frac{1}{\rho}\frac{\partial \psi}{\partial z} = \frac{\partial \phi}{\partial \rho} \quad \text{at} \quad z = 0, \tag{4.13}$$

together with the impermeability and no-slip conditions on the particle boundary $\mathscr{P}$, which imply that both ψ and its normal derivative vanish there. (The requirement of vanishing tangential derivative on $\mathscr{P}$ necessitates that ψ is a constant on that surface. Because of flow regularity, moreover, $\partial\psi/\partial z$ vanishes on the symmetry axis $\rho = 0$. Thus, ψ must possess the same value on both $\mathscr{E}$ and $\mathscr{P}$.) In addition, the far-field behaviour must comply with velocity decay at infinity, whence $\psi/r^2 \to 0$ there.

It is natural to employ an expansion of the form (3.19) and solve for the leading-order term ψ_0 which satisfies the impermeability and slip conditions on the electrode

$$\psi_0 = 0, \quad \frac{\partial \psi_0}{\partial \xi} = -\frac{2}{\eta}\frac{\partial \phi_0}{\partial \eta} \quad \text{at} \quad \xi = 0 \tag{4.14}$$

together with the impermeability and no-slip conditions on the particle boundary:

$$\psi_0 = 0, \quad \frac{\partial \psi_0}{\partial \xi} = 0 \quad \text{at} \quad \xi = 1. \tag{4.15}$$

A solution of (4.12) which satisfies the far-field decay condition and vanishes at $\xi = 0$ is

$$\psi_0 = \frac{\eta}{(\eta^2 + \xi^2)^{3/2}} \int_0^\infty \{[Q(s) + \xi R(s)] \sinh \xi s + \xi T(s) \cosh \xi s\} J_1(\eta s)\, \mathrm{d}s. \tag{4.16}$$

The coefficients Q, R and T are obtained from the boundary conditions. Thus, the homogeneous conditions (4.15) give

$$[Q(s) + R(s)] \sinh s + R(s) \cosh s = 0, \tag{4.17}$$

$$s\,Q(s)\, \cosh s + s R(s)\, \cosh s + s T(s)\, \sinh s - Q(s)\, \sinh s = 0, \tag{4.18}$$

while the inhomogeneous slip condition (4.14), in conjunction with the known properties of the Hankel transform, yields

$$s\,Q(s) + T(s) = -2s\frac{\mathrm{d}^2 A}{\mathrm{d}s^2}. \tag{4.19}$$

Note that at this stage, with $A(s)$ known, (4.17)–(4.19) constitutes a linear algebraic system for Q, R and T; the solution of (4.17)–(4.19) is provided in the Appendix.

At large distances from the particle, $r \to \infty$, where both ξ and η are $O(1/r)$, the integral transform (4.16) becomes

$$\psi_0 \sim \frac{\eta}{(\eta^2 + \xi^2)^{3/2}} \left[\eta\xi\, \mathscr{I}^{(0)} + \eta\xi^2 \mathscr{I}^{(1)} + \eta\xi^3 \mathscr{I}^{(2)} + \eta^3 \xi\, \mathscr{I}^{(3)} + O(r^{-5})\right], \tag{4.20}$$

wherein

$$\left.\begin{aligned} \mathscr{I}^{(0)} &= \frac{1}{2}\int_0^\infty s[s\,Q(s) + T(s)]\, \mathrm{d}s, \quad \mathscr{I}^{(1)} = \frac{1}{2}\int_0^\infty s^2 R(s)\, \mathrm{d}s, \\ \mathscr{I}^{(2)} &= \frac{1}{12}\int_0^\infty s^3[s\,Q(s) + 3T(s)]\, \mathrm{d}s, \quad \mathscr{I}^{(3)} = -\frac{1}{16}\int_0^\infty s^3[s\,Q(s) + T(s)]\, \mathrm{d}s. \end{aligned}\right\} \tag{4.21}$$

Substitution of (4.17)–(4.19) yields $\mathscr{I}^{(0)} = 0$ and $\mathscr{I}_3 = -\pi^4/120$. In addition, numerical quadrature of (4.21) using (A 1) yields $\mathscr{I}^{(1)} \doteqdot -0.84563$ and $\mathscr{I}^{(2)} \doteqdot 2.808$.

https://doi.org/10.1017/S0022112009992631 Published online by Cambridge University Press

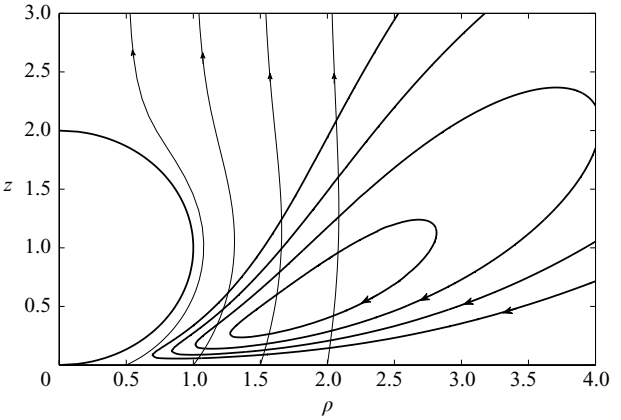


FIGURE 4. Outer solution near the anode in the meridian plane: electric field lines (thin) and electro-hydrodynamic streamlines (thick).

Reverting to spherical coordinates yields

$$\psi_0 \sim 2\mathscr{I}^{(1)}\frac{\cos^2\theta\sin^2\theta}{r} + 4\mathscr{I}^{(2)}\frac{\cos^3\theta\sin^2\theta}{r^2} + 4\mathscr{I}^{(3)}\frac{\cos\theta\sin^4\theta}{r^2} + O(r^{-3}). \quad (4.22)$$

Thus, the leading-order velocity decays like $1/r^3$, just as the electric current disturbance due to the particle presence. Notice however that the first two terms in (4.22) do not contribute to the velocity on the electrode ($\theta = \pi/2$, where $r = \rho$), which therefore decays as $1/r^4$. Indeed, the radial velocity is

$$-\frac{1}{r^2\sin\theta}\frac{\partial\psi_0}{\partial\theta}\bigg|_{\theta=\pi/2} \sim -\frac{\pi^4}{30r^4} + O(r^{-5}) \quad \text{for} \quad r \gg 1, \quad (4.23)$$

in agreement with (2.11) and (3.30). The inward direction of this slip velocity is consistent with the observed aggregation mechanism.

Using the small-s behaviour of Q, R and T readily provides the singular behaviour of ψ near the origin, where $\eta \to \infty$:

$$\psi_0 \sim -2\frac{\xi(1-\xi)^2}{\eta^2}. \quad (4.24)$$

Comparison with the inner expression (4.11) in conjunction of (4.2) verifies that the van Dyke 1–1 matching rule is automatically satisfied.

The streamlines associated with the electro-hydrodynamic flow (4.16) in the outer region are portrayed in figure 4. Also shown are the electric field lines, obtained using (3.21). Note the similarity of the streamlines to those in figure 4(b) of Ristenpart *et al.* (2007*a*).

5. Flow due to particle-animated slip

Consider now the superimposed effect of a non-zero particle zeta potential, resulting in the electro-osmotic flow ($\tilde{\boldsymbol{u}}$, $\tilde{p}$). As with the electro-hydrodynamic flow calculation of the preceding section, the analysis is performed in both the inner and outer regions.

https://doi.org/10.1017/S0022112009992631 Published online by Cambridge University Press

5.1. *Inner region*

The scaling (4.1) is re-employed. Thus, the leading-order fields $\tilde{U}_0$, $\tilde{W}_0$ and $\tilde{P}_0$ are governed by (4.4)–(4.5). The boundary conditions, however, differ from those in §4.1: here both $\tilde{U}_0$, $\tilde{W}_0$ vanish at $Z = 0$, while on the particle boundary they satisfy the conditions (cf. (2.16))

$$\tilde{U}_0 = \frac{\mathrm{d}\varphi_0}{\mathrm{d}R} \quad \text{at} \quad Z = H_0 \tag{5.1}$$

and

$$\tilde{W}_0 = \frac{\partial\varphi_1}{\partial Z} - 1 \quad \text{at} \quad Z = H_0. \tag{5.2}$$

The radial momentum balance in conjunction with (3.13) and (5.1) readily yields (cf. (4.7))

$$\tilde{U}_0 = \frac{1}{2}\frac{\mathrm{d}\tilde{P}_0}{\mathrm{d}R} Z(Z - H_0) - \frac{RZ}{2H_0^2}. \tag{5.3}$$

Calculation of $\tilde{W}_0$ in conjunction with (3.10) and (5.2) shows that $\tilde{P}_0$ satisfies (4.8), whence

$$\tilde{P}_0 = P_0. \tag{5.4}$$

The stream function corresponding to the leading-order flow is readily found to be

$$\tilde{\Psi}_0 = \frac{R^2 Z^2}{2H_0^3}(H_0 - Z^2). \tag{5.5}$$

5.2. *Outer flow*

The stream function $\tilde{\psi}$ is related to $\tilde{\boldsymbol{u}}$ through relations of the form (2.18). Thus, $\tilde{\psi}$ is also governed by (4.12), but now with impermeability and no-slip conditions on $\mathscr{E}$ (whereby both the stream function and its normal derivative vanish there) together with impermeability and slip conditions on $\mathscr{P}$. Expressed in tangent-sphere coordinates, the leading-order boundary conditions appear as

$$\tilde{\psi}_0 = 0, \quad \frac{\partial\tilde{\psi}_0}{\partial\xi} = 0 \quad \text{at} \quad \xi = 0, \tag{5.6a, b}$$

and

$$\tilde{\psi}_0 = 0, \qquad \frac{\partial\tilde{\psi}_0}{\partial\xi} = -\frac{2\eta}{1+\eta^2}\frac{\partial\phi_0}{\partial\eta} - \frac{8\eta^2}{(1+\eta^2)^3} \quad \text{at} \quad \xi = 1. \tag{5.7a, b}$$

Just like ψ_0, $\tilde{\psi}_0$ is governed by (4.12), vanishes at $\xi = 0$, and is $o(1/r^2)$ at large r. Thus, it possesses the solution (4.16) with Q, R ,and T replaced by different coefficients, say $\tilde{Q}$, $\tilde{R}$, and $\tilde{T}$. This solution automatically satisfies (5.6*a*), whereas the remaining homogeneous condition at $\xi = 0$, (5.6*b*), adopts the form

$$s\,\tilde{Q}(s) + \tilde{T}(s) = 0. \tag{5.8}$$

At $\xi = 1$, the impermeability condition (5.7*a*) reads

$$[\tilde{Q}(s) + \tilde{R}(s)]\sinh s + \tilde{R}(s)\cosh s = 0, \tag{5.9}$$

while the inhomogeneous slip condition (5.7*b*) is readily transformed to the equation

$$\tilde{R}(s)\sinh s + s\tilde{R}(s)\cosh s + s\tilde{T}(s)\sinh s = -2s\frac{\mathrm{d}^2 A}{\mathrm{d}s^2}\cosh s - 4s\frac{\mathrm{d}A}{\mathrm{d}s}\sinh s - 8s\mathrm{e}^{-s}. \tag{5.10}$$

https://doi.org/10.1017/S0022112009992631 Published online by Cambridge University Press

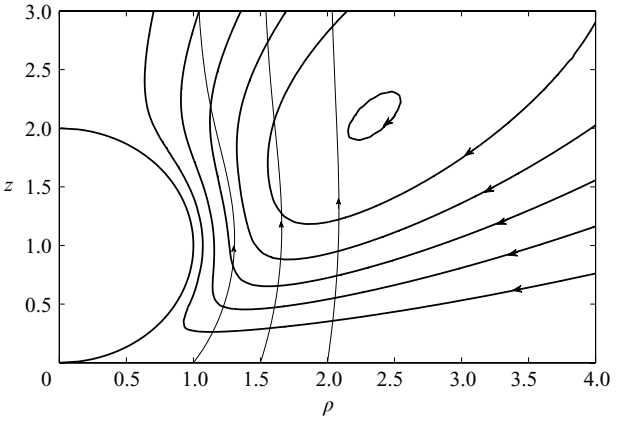


FIGURE 5. Outer solution near the anode in the meridian plane: electric field lines (thin) and electro-osmotic streamlines (thick). The flow direction corresponds to a negative particle zeta potential ($\chi < 0$).

The solution of the linear system (5.8)–(5.10) is provided in the Appendix.

As with the electro-hydrodynamic flow, the solution allows for analytic approximations at various regions. Thus, at large distances from the particle $\tilde{\psi}_0$ is provided by an expression of the form (4.20),

$$\tilde{\psi}_0 \sim \frac{\eta}{(\eta^2+\xi^2)^{3/2}}\left[\eta\xi\,\tilde{\mathscr{F}}^{(0)} + \eta\xi^2\,\tilde{\mathscr{F}}^{(1)} + \eta\xi^3\,\tilde{\mathscr{F}}^{(2)} + \eta^3\xi\,\tilde{\mathscr{F}}^{(3)} + O(r^{-5})\right]. \tag{5.11}$$

Here, $\tilde{\mathscr{F}}^{(0)}$, $\tilde{\mathscr{F}}^{(1)}$, $\tilde{\mathscr{F}}^{(2)}$ and $\tilde{\mathscr{F}}^{(3)}$ are provided by relations of the form (4.21), in which with Q, R and T are replaced by $\tilde{Q}$, $\tilde{R}$ and $\tilde{T}$. In view of (5.8), both $\tilde{\mathscr{F}}^{(0)}$ and $\tilde{\mathscr{F}}^{(3)}$ vanish here. Also, numerical quadrature using (A 2) yields

$$\tilde{\mathscr{F}}^{(1)} \doteqdot 8.11163, \quad \tilde{\mathscr{F}}^{(2)} \doteqdot -10.8082. \tag{5.12}$$

Summarizing, the leading-order outer flow field decays as r^{-3},

$$\tilde{\psi}_0 \sim 2\tilde{\mathscr{F}}^{(1)}\frac{\cos^2\theta\sin^2\theta}{r} + 4\tilde{\mathscr{F}}^{(2)}\frac{\cos^3\theta\sin^2\theta}{r^2} + O(r^{-3}), \tag{5.13}$$

just like that due to the flow associated with electrode-animated slip. Of course, this flow field vanishes on the electrode, in view of the boundary condition which is satisfied by $\tilde{\boldsymbol{u}}$ there.

The singular behaviour of the outer flow is obtained using the small-s behaviour of $\tilde{Q}$, $\tilde{R}$ and $\tilde{T}$, thereby yielding

$$\tilde{\psi}_0 \sim 2\frac{\xi^2(1-\xi)}{\eta^2}. \tag{5.14}$$

Comparison with (5.5) in conjunction with (4.2) verifies that the van Dyke 1–1 matching rule is automatically satisfied.

The streamlines $\tilde{\psi}_0 =$ constant, associated with the electro-osmotic flow in the outer region, are portrayed in figure 5. Also shown are the electric field lines, obtained using (3.21). Note the similarity of the streamlines to those in figure 4(a) of Ristenpart *et al.* (2007*a*).

https://doi.org/10.1017/S0022112009992631 Published online by Cambridge University Press

6. Results

With the electric and flow field evaluated, it is now possible to calculate two quantities which are of interest in understanding the particle clustering phenomena.

6.1. *Particle interaction*

The velocity field $\boldsymbol{v}$ generated by the particle may be exploited to calculate the consequent drift of a neighbouring identical particle. The hydrodynamic force acting on the latter, normalized with $6\pi\mu a\mathscr{U}$, is provided by Faxén's law (Happel & Brenner 1965):

$$\boldsymbol{v} + \frac{1}{6}\nabla^2\boldsymbol{v} \tag{6.1}$$

applied at the location of the neighbouring particle centre. To apply this formula, it is useful to obtain an asymptotic approximation for the flow field near the electrode at large distances from the particle. This remote region is naturally expressed using cylindrical coordinates, whereby focus lies in the limit

$$\rho \to \infty \quad \text{while} \quad z = O(1). \tag{6.2}$$

Note that the previously obtained far-field limit for $r \to \infty$ is not directly applicable for that purpose, since the asymptotic expansion (4.20) is non-uniform for $\theta \to \pi/2$. The delicate approach to large distances is evident in the tangent-sphere coordinates (2.22), wherein (6.2) is transformed to

$$\eta = O(\rho^{-1}), \quad \xi = O(\rho^{-2}). \tag{6.3}$$

Consider first the electro-hydrodynamic flow. Applying the limit (6.3) to the integral representation (4.16) of ψ_0 yields

$$\psi_0 \sim \frac{\xi}{\eta}\left[\mathscr{I}^{(0)} + \mathscr{I}^{(1)}\xi + \mathscr{I}^{(3)}\eta^2 + O(\xi^2, \eta^4)\right]. \tag{6.4}$$

Note the difference with (4.20). Since $\mathscr{I}^{(0)} = 0$, (6.4) provides a single leading-order term in an asymptotic expansion at inverse powers of ρ, obtained via use of (2.22):

$$\psi_0 \sim \frac{2\mathscr{I}^{(1)}z^2 + 4\mathscr{I}^{(3)}z}{\rho^3} + O(\rho^{-5}). \tag{6.5}$$

The respective radial velocity component (see (2.17)) is provided using (2.18):

$$u_0 \sim 4\frac{\mathscr{I}^{(1)}z + \mathscr{I}^{(3)}}{\rho^4} + O(\rho^{-6}). \tag{6.6}$$

The contribution of the second term in (6.1) in the radial direction is

$$\left[1 + O(\rho^{-2})\right]\frac{\partial^2 u_0}{\partial z^2} \sim O(\rho^{-6}). \tag{6.7}$$

Thus, (6.6) constitutes a leading-order approximation for the radial force on a neighbouring particle. The velocity component w_0 in the z direction, away from the electrode, is only $O(\rho^{-5})$.

The preceding analysis also applies for the electro-osmotic flow. Here, because $\tilde{\mathscr{I}}^{(3)} = 0$, only one term appears in the leading-order approximation for the radial velocity

$$\tilde{u}_0 \sim \frac{4\tilde{\mathscr{I}}^{(1)}z}{\rho^4} + O(\rho^{-6}). \tag{6.8}$$

https://doi.org/10.1017/S0022112009992631 Published online by Cambridge University Press

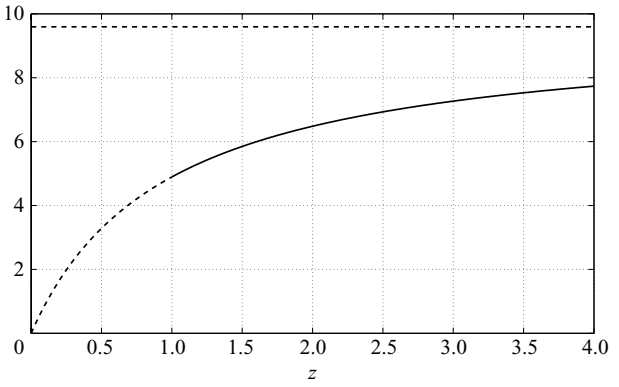


FIGURE 6. The ratio $-\tilde{u}_0/u_0$ at large ρ as a function of distance z from the electrode. The solid part of the curve represents the relevant z values for the position of a neighbouring particle. The dashed horizontal line is the large-z asymptote $\tilde{u}_0/u_0 = \tilde{\mathscr{F}}^{(1)}/\mathscr{F}^{(1)}$.

This expression vanishes at $z = 0$, as it must.

The ρ^{-4} decay rate was actually observed by Ristenpart *et al.* (2007*a*), who employed reflection arguments to explain it (Ristenpart *et al.* 2007*a*,*b*). Such arguments however can only provide the behaviour in the limit $r \to \infty$ and are not appropriate to the limit (6.2). Indeed, the leading-order velocity 6.6 is actually associated with a term that decays like $1/r^3$.

The interaction approximations (6.6) and (6.8) allow for a rough comparison between the electro-hydrodynamic and electro-osmotic contributions to the attractive force in the radial direction. It is natural to perform this comparison for identical magnitude of the particle and anode zeta potential. Considering as usual $\zeta_P < 0$, this implies $\chi = -1$. Thus, the relative magnitude of the electro-osmotic contribution to the force, compared with the respective electro-hydrodynamic contribution, is provided by the ratio

$$-\frac{\tilde{u}_0}{u_0} \sim -\frac{\tilde{\mathscr{F}}^{(1)} z}{\mathscr{F}^{(1)} z + \mathscr{F}^{(3)}}, \tag{6.9}$$

which is portrayed in figure 6 as a function of z. Note that only the values $z > 1$ are relevant for the location of a neighbouring particle centre. For these values, the force ratio is larger than unity, implying practical dominance of the electro-osmotic contribution. If the neighbouring particle is also nearly touching the electrode, whereby $z \approx 1$, the ratio approaches its minimal value $-\tilde{\mathscr{F}}^{(1)}/(\mathscr{F}^{(3)} + \mathscr{F}^{(1)}) \doteqdot 4.8943$. At large values of z (which must be small compared with ρ), the ratio attains its maximum asymptotic value $-\tilde{\mathscr{F}}^{(1)}/\mathscr{F}^{(1)} \doteqdot 9.5924$.

6.2. *Levitation mechanism*

The other quantity of interest is the force experienced by the particle. In both the electro-osmotic and electro-hydrodynamic flows the pressure in the gap region is $O(\delta^{-2})$ large. Since this pressure acts upon an $O(\delta)$ area, it results in an $O(\delta^{-1})$ contribution to the hydrodynamic force. This contribution clearly dominates the complementary contribution of the outer region, wherein the hydrodynamic stress is $O(1)$. Thus, the hydrodynamic force (normalized with $\mu a \mathscr{U}$) which is contributed by the superposition of $\boldsymbol{u}$ and $\chi\tilde{\boldsymbol{u}}$ is approximately given by $\delta^{-1}F$, where F is contributed

https://doi.org/10.1017/S0022112009992631 Published online by Cambridge University Press

from the inner pressure field. In view of (5.4):

$$F = 2\pi(1+\chi)\int_0^\infty P_0(R)R\,\mathrm{d}R. \tag{6.10}$$

Substitution of (4.10) readily yields $F = 3\pi(1+\chi)$.

In addition to the hydrodynamic force, the particle also experiences an electric force, provided by surface quadrature of Maxwell stresses. These stresses are quadratic in the electric field and are therefore $O(1)$ in the outer region and $O(\delta^{-1})$ in the inner one; while still large in the narrow gap, their contribution is subdominant to that of the pressure forces. Thus, the equilibrium position of the particle is essentially set up by the balance between the hydrodynamic force and (the difference between the) gravity and buoyancy forces. In the reported experiments the particle zeta potential is negative, but is smaller in absolute value from the electrode zeta potential (Fagan *et al.* 2004): $0 < 1+\chi < 1$. Thus, the main effect of particle charge is to reduce the repulsive hydrodynamic force. For a freely suspended particle, this results in a smaller value of δ at the equilibrium position. In view of the δ-dependence of the hydrodynamic force, this is statically stable equilibrium.

7. Concluding remarks

In summary, this investigation exploited the smallness of the gap width in the particle–electrode interaction to obtain an asymptotic approximation for the electro-kinetic processes which occur as a result of a uniform DC ionic current which is emitted out of the electrode. While the gap smallness has been numerically implicit in previous analysis of the problem, this is the first time where it is used explicitly. In my opinion, the present asymptotic approach is not only the conceptually correct procedure to analyse that problem, but is also the only way that can resolve the singular gap region. As seen in the previous section, the large pressure field in that region is actually responsible to the leading-order hydrodynamic force on the particle, which tends to repel it away from the wall. When Debye layer overlap does occur, the thin-Debye-layer model is inapplicable in the gap region. In these circumstances, DLVO forces may actually lead to particle–wall adhesion.

In the outer region, outside the narrow gap, the present analysis provides the electro-hydrodynamic and electro-osmotic flow components in the form of integral transforms. Asymptotic approximation of these components at large distance reveals that the velocity field decays with the third power of that distance. Near the electrode, however, the velocity decays with the fourth power: this is the mechanism which leads to effective particle attraction. For equal zeta potentials, it is found that the electro-osmotic contribution to the attraction dominates the respective electro-hydrodynamic contribution by a factor which ranges roughly between five and ten. Conversely, this factor represents the large electrode zeta potential which is required for comparable contributions. The bipolar-coordinates calculations of Ristenpart *et al.* (2007*a*) were based upon a zeta-potential ratio of about eight; at this large ratio, both contributions were indeed found comparable (see figure 5 in Ristenpart *et al.* 2007*a*). (The large anode-zeta-potential values used in the Ristenpart *et al.* (2007*a*) simulations correspond to (half of) the reported values of applied electrodes voltage in existing experiments (Solomentsev *et al.* 2000), thereby neglecting the voltage drop in the Ohmic bulk.)

https://doi.org/10.1017/S0022112009992631 Published online by Cambridge University Press

It is worthwhile at this point to emphasize the major approximations in this paper: (i) the Debye thickness is small compared with the particle–electrode gap, itself small compared with the particle size; (ii) on the bulk scale, the electrode is equivalent to a uniformly prescribed surface current; and (iii) the zeta potential on the electrode is uniform, unaffected by the particle presence. While the first assumption is clearly supported by typical experimental figures (see table 1), the latter two may constitute a rather crude approximation. Nevertheless, these two assumptions represent the state-of-the art modelling in the field.

A more accurate model requires a systematic thin-Debye-layer asymptotic analysis of electrokinetic phenomena which are driven by ion-exchange surfaces, similar to the comparable analyses of electrokinetic phenomena in the presence of inert surfaces (Keh & Anderson 1985; Cox 1997; Yariv 2010). Existing asymptotic analyses of reactive electrodes that explicitly take into account the electrode kinetics (Rubinstein & Shtilman 1979; Bazant *et al.* 2005) tend to focus upon one-dimensional transport processes. As such, they are inadequate for the present problem. (Clearly, no mass flow is present in these one-dimensional models.) Because the one-dimensional ionic transport may be unstable, these models have been generalized to handle three-dimensional transport processes, whereby electrolyte flow may occur (Rubinstein, Zaltzman & Kedem 1997; Rubinstein & Zaltzman 2000; Zaltzman & Rubinstein 2007). Nonetheless, these generalized models are unsuitable to handle flow fields which are imposed by the presence of curved inert surfaces of arbitrary shape (e.g. the boundary of a colloidal particle).

To be applicable to the present problem, the preceding analyses should be extended to handle more general (non-one-dimensional) geometries. Such geometries constitute a conceptual difficulty as compared to the one-dimensional analyses. Consider indeed the pertinent length scales involved: The one-dimensional geometries are characterized by two length scales: λ, the Debye thickness and h, the electrode spacing; inspection of more general geometry, on the other hand, introduces two more length scales: a, a characteristic particle size and $a\delta$, particle–electrode separation. While the analysis of such a multi-scale problem appears formidable, it could possibly be carried out using the inherent scale disparity in the problem. If succeeded, it can extract the desired macro-scale electrode model from the microscale physics, relating the current-density and zeta-potential distributions on the anode to the experimental controlled problem inputs: the electrodes voltage, the electrode kinetics and the dimensions of the electro-chemical cell.

Appendix. Solutions of linear systems

The solution of (4.17)–(4.19) is

$$\left.\begin{aligned} Q &= -\frac{32\mathrm{e}^{4s}s^2(2s+\mathrm{e}^{2s}(2s-3)+3)}{(\mathrm{e}^{2s}-1)^3(\mathrm{e}^{4s}-2\mathrm{e}^{2s}(2s^2+1)+1)},\\ R &= -\frac{8\mathrm{e}^{2s}s(\mathrm{e}^{6s}(2s-3)+\mathrm{e}^{2s}(3-8s^2-14s)+\mathrm{e}^{4s}(3-8s^2+14s)-2s-3)}{(\mathrm{e}^{2s}-1)^3(\mathrm{e}^{4s}-2\mathrm{e}^{2s}(2s^2+1)+1)},\\ T &= \frac{8\mathrm{e}^{2s}s(2s+\mathrm{e}^{2s}(2s-3)+3)}{(\mathrm{e}^{2s}-1)(\mathrm{e}^{4s}-2\mathrm{e}^{2s}(2s^2+1)+1)}. \end{aligned}\right\} \quad (A\,1)$$

https://doi.org/10.1017/S0022112009992631 Published online by Cambridge University Press

The solution of (5.8)–(5.10) is

$$\left.\begin{aligned} \tilde{Q} &= \frac{4s(2s\,\mathrm{csch}^2 s - 3\,\coth s)}{2s^2 - \cosh 2s + 1}, \\ \tilde{R} &= -\frac{2s\,\mathrm{csch}^3 s(s\,\cosh s - \sinh s)(3\,\sinh 2s - 4s)}{2s^2 - \cosh 2s + 1}, \\ \tilde{T} &= \frac{4s^2(3\,\coth s - 2s\,\mathrm{csch}^2 s)}{2s^2 - \cosh 2s + 1}. \end{aligned}\right\} \tag{A 2}$$

REFERENCES

Bazant, M. Z., Chu, K. T. & Bayly, B. J. 2005 Current-voltage relations for electrochemical thin films. *SIAM J. Appl. Math.* **65**, 1463–1484.

Bazant, M. Z. & Squires, T. M. 2004 Induced-charge electrokinetic phenomena: theory and microfluidic applications. *Phys. Rev. Lett.* **92**, 066101.

Böhmer, M. 1996 In situ observation of 2-dimensional clustering during electrophoretic deposition. *Langmuir* **12**, 5747–5750.

Cox, R. G. 1997 Electroviscous forces on a charged particle suspended in a flowing liquid. *J. Fluid Mech.* **338**, 1–34.

Cox, R. G. & Brenner, H. 1967 The slow motion of a sphere through a viscous fluid towards a plane surface – II. Small gap widths, including inertial effects. *Chem. Engng Sci.* **22**, 1753–1777.

Dukhin, S. S. 1965 Diffusion-electrical theory of electrophoresis. In *Twentieth Intl Cong. on Pure and Applied Chemistry*, vol. A72, p. 68, Moscow.

van Dyke, M. 1964 *Perturbation Methods in Fluid Mechanics*. Academic Press.

Fagan, J. A., Sides, P. J. & Prieve, D. C. 2002 Vertical oscillatory motion of a single colloidal particle adjacent to an electrode in an ac electric field. *Langmuir* **18**, 7810–7820.

Fagan, J. A., Sides, P. J. & Prieve, D. C. 2004 Vertical motion of a charged colloidal particle near an AC polarized electrode with a non-uniform potential distribution: theory and experimental evidence. *Langmuir* **20**, 4823–4834.

Fagan, J. A., Sides, P. J. & Prieve, D. C. 2006 Mechanism of rectified lateral motion of particles near electrodes in alternating electric fields below 1 kHz. *Langmuir* **22**, 9846–9852.

Goldman, A. J., Cox, R. & Brenner, H. 1967 Slow viscous motion of a sphere parallel to a plane wall – I. Motion through a quiescent fluid. *Chem. Engng Sci.* **22**, 637–651.

Gong, T. & Marr, D. W. M. 2001 Electrically switchable colloidal ordering in confined geometries. *Langmuir* **17**, 2301–2304.

Happel, J. & Brenner, H. 1965 *Low Reynolds Number Hydrodynamics*. Prentice-Hall.

Hinch, E. J. 1991 *Perturbation Methods*. Cambridge University Press.

Jeffrey, D. J. 1978 The temperature field or electric potential around two almost touching spheres. *J. Inst. Math. Appl.* **22**, 337–351.

Jeffrey, D. J. & Chen, H. S. 1977 The virtual mass of a sphere moving towards a plane wall. *J. Appl. Mech.* **44**, 166–167.

Keh, H. J. & Anderson, J. L. 1985 Boundary effects on electrophoretic motion of colloidal spheres. *J. Fluid Mech.* **153**, 417–439.

Keh, H. J. & Lien, L. C. 1989 Electrophoresis of a dielectric sphere normal to a large conducting plane. *J. Chin. Inst. Chem. Engng* **20**, 283–290.

Keller, J. B. 1963 Conductivity of a medium containing a dense array of perfectly conducting spheres or cylinders or nonconducting cylinders. *J. Appl. Phys.* **34**, 991–993.

Kim, J., Anderson, J. L., Garoff, S. & Sides, P. J. 2002*a* Effects of zeta potential and electrolyte on particle interactions on an electrode under ac polarization. *Langmuir* **18** (14), 5387–5391.

Kim, J., Guelcher, S. A., Garoff, S. & Anderson, J. L. 2002*b* Two-particle dynamics on an electrode in ac electric fields. *Adv. Colloid Interface* **96**, 131–142.

Levich, V. G. 1962 *Physicochemical Hydrodynamics*. Prentice-Hall.

https://doi.org/10.1017/S0022112009992631 Published online by Cambridge University Press

Loewenberg, M. & Davis, R. H. 1995 Near-contact electrophoretic particle motion. *J. Fluid Mech.* **288**, 103–122.

Lumsdon, S. O., Kaler, E. W., Williams, J. P. & Velev, O. D. 2003 Dielectrophoretic assembly of oriented and switchable two-dimensional photonic crystals. *Appl. Phys. Lett.* **82**, 949–951.

Moon, P. & Spencer, D. E. 1988 *Field Theory Handbook*. Springer.

Nadal, F., Argoul, F., Hanusse, P., Pouligny, B. & Ajdari, A. 2002 Electrically induced interactions between colloidal particles in the vicinity of a conducting plane. *Phys. Rev.* E **65** (6), 61409.

Newman, J. S. 1973 *Electrochemical Systems*. Prentice-Hall.

O'Brien, R. W. 1983 The solution of the electrokinetic equations for colloidal particles with thin double layers. *J. Colloid Interface Sci.* **92** (1), 204–216.

Reed, L. D. & Morrison, F. A. 1976 Hydrodynamic interactions in electrophoresis. *J. Colloid Interface Sci.* **54**, 117–133.

Ristenpart, W. D., Aksay, I. A. & Saville, D. A. 2004 Assembly of colloidal aggregates by electrohydrodynamic flow: kinetic experiments and scaling analysis. *Phys. Rev.* E **69**, 21405.

Ristenpart, W. D., Aksay, I. A. & Saville, D. A. 2007*a* Electrically driven flow near a colloidal particle close to an electrode with a Faradaic current. *Langmuir* **23**, 4071–4080.

Ristenpart, W. D., Aksay, I. A. & Saville, D. A. 2007*b* Electrohydrodynamic flow around a colloidal particle near an electrode with an oscillating potential. *J. Fluid Mech.* **575**, 83–109.

Rubinstein, I. & Shtilman, L. 1979 Voltage against current curves of cation exchange membranes. *J. Chem. Soc. Faraday Trans. 2* **75**, 231–246.

Rubinstein, I. & Zaltzman, B. 2000 Electro-osmotically induced convection at a permselective membrane. *Phys. Rev.* E **62**, 2238–2251.

Rubinstein, I. & Zaltzman, B. 2001 Electro-osmotic slip of the second kind and instability in concentration polarization at electrodialysis membranes. *Math. Models Methods Appl. Sci.* **11**, 263–300.

Rubinstein, I., Zaltzman, B. & Kedem, O. 1997 Electric fields in and around ion-exchange membranes. *J. Membr. Sci.* **125**, 17–21.

Russel, W. B., Saville, D. A. & Schowalter, W. R. 1989 *Colloidal Dispersions*. Cambridge University Press.

Sides, P. J. 2001 Electrohydrodynamic particle aggregation on an electrode driven by an alternating electric field normal to it. *Langmuir* **17**, 5791–5800.

Sides, P. J. 2003 Calculation of electrohydrodynamic flow around a single particle on an electrode. *Langmuir* **19**, 2745–2751.

Sides, P. J. & Tobias, C. W. 1980 Primary potential and current distribution around a bubble on an electrode. *J. Electrochem. Soc.* **127**, 288–291.

Sneddon, I. N. 1972 *The Use of Integral Transforms*. McGraw-Hill.

Solomentsev, Y., Böhmer, M. & Anderson, J. L. 1997 Particle clustering and pattern pormation during electrophoretic deposition: a hydrodynamic model. *Langmuir* **13**, 6058–6068.

Solomentsev, Y., Guelcher, S. A., Bevan, M. & Anderson, J. L. 2000 Aggregation dynamics for two particles during electrophoretic deposition under steady fields. *Langmuir* **16**, 9208–9216.

Squires, T. M. & Bazant, M. Z. 2004 Induced-charge electro-osmosis. *J. Fluid Mech.* **509**, 217–252.

Trau, M., Saville, D. A. & Aksay, I. A. 1996 Field-induced layering of colloidal crystals. *Science* **272**, 706.

Trau, M., Saville, D. A. & Aksay, I. A. 1997 Assembly of colloidal crystals at electrode interfaces. *Langmuir* **13**, 6375–6381.

Velev, O. & Kaler, E. 1999 In situ assembly of colloidal particles into miniaturized biosensors. *Langmuir* **15**, 3693–3698.

Wong, E. M. & Searson, P. C. 1999 ZnO quantum particle thin films fabricated by electrophoretic deposition. *Appl. Phys. Lett.* **74**, 2939–2941.

Yariv, E. 2008 Nonlinear electrophoresis of ideally polarizable spherical particles. *Europhys. Lett.* **82**, 54004.

Yariv, E. 2010 An asymptotic derivation of the thin-Debye-layer limit for electrokinetic phenomena. *Chem. Engng Commun.* **197**, 3–17.

Zaltzman, B. & Rubinstein, I. 2007 Electro-osmotic slip and electroconvective instability. *J. Fluid Mech.* **579**, 173–226.

https://doi.org/10.1017/S0022112009992631 Published online by Cambridge University Press